Pergamon

Bioorganic & Medicinal Chemistry, Vol. 5, No. 1, pp 93–99, 1997

PII: S0968-0896(96)00205-2
0968-0896/97 $17.00 + 0.00

Antitumor 8-Chlorobenzocycloheptapyridines: a New Class of Selective, Nonpeptidic, Nonsulfhydryl Inhibitors of Ras Farnesylation

A. K. Mallams, F. G. Njoroge, R. J. Doll,* M. E. Snow, J. J. Kaminski, R. R. Rossman, B. Vibulbhan, W. R. Bishop, P. Kirschmeier, M. Liu, M. S. Bryant, C. Alvarez, D. Carr, L. James, I. King, Z. Li, C.-C. Lin, C. Nardo, J. Petrin, S. W. Remiszewski, A. G. Taveras, S. Wang, J. Wong, J. Catino, V. Girijavallabhan and A. K. Ganguly

Schering-Plough Research Institute, 2015 Galloping Hill Road, Kenilworth, NJ 07033, U.S.A.

Abstract—Ras farnesylation by farnesyl protein transferase (FPT) is an intracellular event that facilitates the membrane association of the ras protein and is involved in the signal transduction process. FPT inhibition could be a novel, noncytotoxic method of treating ras dependent tumor growth. We report here three structural classes of 8-chlorobenzocycloheptapyridines as novel, nonpeptidic, nonsulfhydryl FPT inhibitors having antitumor activity in mice when dosed orally. We discuss structural and conformational aspects of these compounds in relation to biological activities as well as a comparison to the conformation of a bound tetrapeptide FPT inhibitor. Copyright © 1997 Elsevier Science Ltd

Introduction

Ras proteins play an important role in the signal transduction processes involved in cell division.[1] Recently, several steps in this signal transduction process have been elucidated.[2] Point mutations in the ras genes (H-, N- and K-ras) that encode the ras proteins have been observed in ~30% of all human cancers.[3] Ras proteins undergo a series of post-translationational modifications which include the farnesylation of ras by farnesyl protein transferase (FPT).[4,5] These modifications result in cell membrane association which is necessary for ras to exhibit biological activity. Consequently, the inhibition of FPT has been the subject of intense study over the last few years. This resulted in the development of a number of structural types that are potent inhibitors of FPT, in vitro tumor cell growth, and tumor growth in animals.[6–8] However, most of the reported FPT inhibitors are peptidic or peptidomimetic, and contain free amino and sulfhydryl groups which are potentially metabolically labile. Recently, this laboratory reported on a novel tricyclic FPT inhibitor, SCH 44342 (Scheme 1), featuring an 8-chlorobenzocycloheptapyridine moiety.[9] SCH 44342 is unique since it is nonpeptidic, is selective for FPT over GGPT (geranylgeranyl protein transferase),[10,11] does not contain a sulfhydryl group, and kinetically competes with the ras protein but not with farnesyl pyrophosphate in binding to FPT. We wish to disclose additional novel compounds in this 8-chloro-5,6-dihydro-11*H*-benzo[5,6]cyclohepta[1,2-*b*] pyridine structural class which are potent inhibitors of FPT. The effects of stereochemical and structural modifications of these inhibitors on enzyme, cellular and in vivo antitumor activities are discussed. Also, a Catalyst-generated hypothesis[12] has been developed and its correlation to the NMR-determined bound conformation of a peptide FPT inhibitor[13,14] is described.

Synthesis

The three structural classes, represented by SCH 44342, SCH 55495 (Scheme 1) and SCH 54429 (Scheme 2), differ in the central six-membered heterocyclic ring and the nature of the bond joining this ring to the 8-chlorobenzocycloheptapyridine substituent. SCH 44342, prepared from amine **1**,[15] where a piperidine substituent is attached to the tricyclic moiety by an unsaturated bond, has been previously described.[15] The carbonyl transposed isomer, SCH 50739, was prepared by alkylation of amine **1** with 4-(2-bromoacetyl)pyridine. Lithium aluminum hydride reduction of the olefin in **1** provided piperidine **2** (along with the 8-dechloro material) which, when coupled with 4-pyridylacetic acid hydrochloride using 1-(3-dimethylaminopropyl)-3-ethylcarbodiimide hydrochloride (DEC), 1-hydroxybenzotriazole (HOBT), and *N*-methylmorpholine (NMM), afforded SCH 55495 (Scheme 1). Piperazine analogue SCH 54429 was synthesized from racemic **3**[16] and 4-pyridylacetic acid as described for SCH 55495. Resolution of **3** to **4** and **5** prior to coupling with 4-pyridylacetic acid afforded the pure enantiomers *R*(+)-SCH 69955 and *S*(−)-SCH 69956 (Scheme 2).

Results and Discussion

FPT Inhibition

The results of the FPT and GGPT enzyme assays[9] are shown in Table 1. The FPT inhibitory potency of SCH

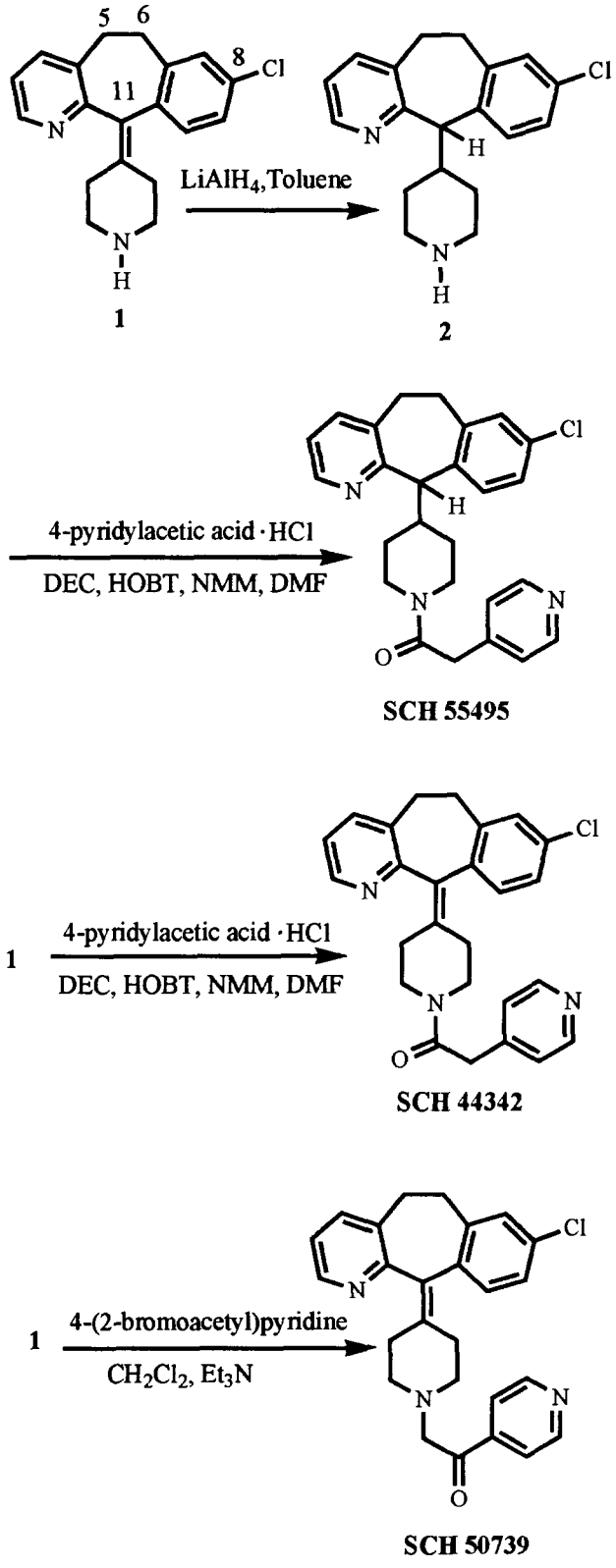

Scheme 1.

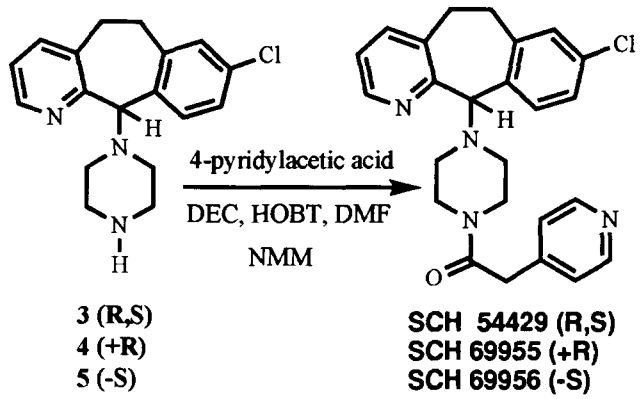

Scheme 2.

44342, racemic SCH 54429 and racemic SCH 55495 were found to be similar. Unlike SCH 44342, sp^3-hybridization at C-11 of SCH 55495 and SCH 54429 imparts additional conformational mobility and asymmetry. The absolute stereochemistry at C-11 is critical since $S(-)$-SCH 69956 and $R(+)$-SCH 69955 were found to differ by a factor of 3.5 in FPT inhibitory potency. Similar compounds in this class (data not shown) are consistent with the enhanced FPT inhibitory potency of the $S(-)$-enantiomer. The importance of the position of the carbonyl group is demonstrated by the diminished FPT inhibitory potency of SCH 50739 compared with SCH 44342. An appropriate acyl substituent as in SCH 44342, SCH 54429 and racemic SCH 55495 is important for FPT inhibition since compounds lacking this moiety (i.e., **1**, **2** and **3**, shown in Schemes 1 and 2) have greatly diminished FPT inhibition. Perhaps, the carbonyl group is acting as a hydrogen-bond acceptor upon interaction with the protein. Fifty percent inhibition of GGPT was not achieved up to 46 μM for the compounds listed in Table 1. The greater than 100-fold selectivity of FPT to GGPT is important since GGPT is a similar enzyme involved in the prenylation and membrane association of other proteins.[10,11] We usually find a potency decrease for FPT inhibition of three to five times for K-ras farnesylation compared to H-ras (data not shown).

Table 1. Enzyme and cellular data for FPT inhibitors. All inhibitions are expressed as IC_{50}s in μM. Details of assays have been previously reported.[9] No data = nd

Compound	FPT	GGPT	Cos
SCH 44342	0.25	>46	1.0
SCH 54429	0.18	>46	3.7
SCH 55495	0.16	>46	1.2
SCH 69955	0.49	nd	nd
SCH 69956	0.14	nd	nd
SCH 50739	15.8	nd	nd
1	>65	nd	nd
2	>65	nd	nd
3	30.3	nd	nd

Table 2. Pharmacokinetic parameters for FPT inhibitors. Compounds dosed at 25 mg/kg in mice as solutions of the hydrochloride salts. Oral = po, intravenous = iv, AUC = area under the concentration–time curve

Compound	$AUC_{0-1\,h}$ (po) (μg h/mL)	Cmax (po) (μg/mL)	$AUC_{0-1\,h}$ (iv) (μg h/mL)	$t_{1/2}$ (iv) (min)
SCH-44342	0.37	1.02	1.75	<10
SCH-54429	0.24	0.40	1.8	<10

Cell-based assay of ras processing

Since ras farnesylation is an intracellular event, we examined the effect of these compounds on ras farnesylation in Cos-7 monkey kidney cells transiently expressing either Ha-Ras-[Val^{12}]CVLS or Ha-Ras-[Val^{12}]CVLL.[9] As is shown Table 1, the IC_{50} for ras farnesylation inhibition in the Cos cell assay by our FPT inhibitors ranged from 1 to 3.7 μM. This is about 10-fold less potent than the FPT enzyme inhibition, and is undoubtedly a function of many parameters including cell penetration.

Pharmacokinetic study

The pharmacokinetics of SCH 44342 and SCH 54429 have been studied and the results are listed in Table 2. In this study, mice were given 25 mg/kg of compound as a single dose either orally (po) or intravenously (iv). Oral administration of SCH 44342 and SCH 54429 produced nearly equivalent AUCs although the Cmax of SCH 44342 was found to be twice that of SCH 54429. The AUCs up to 1 h for these compounds given iv were nearly equivalent and their clearance rates from the serum were found to be less than 10 min.

In vivo antitumor efficacy

We evaluated SCH 44342 and the racemates SCH 54429 and SCH 55495 as antitumor agents, by first growing a human colorectal tumor (SW-620), containing a mutated K-ras, subcutaneously to a size of 100 mm^3 in nude mice. Compounds were then dosed orally as a suspension in corn oil at 100 mg/kg, twice daily for 5 days a week. The rate of tumor growth was monitored and compared with vehicle control. As is seen in Figure 1, SCH 54429 inhibited tumor growth by 42% after 35 days, while SCH 55495 showed a tumor growth inhibition of 18% after 35 days and 30% after 45 days. SCH 44342 showed little tumor growth inhibition under these conditions. Serum pharmacokinetics alone cannot explain the lack of antitumor efficacy of SCH 44342 since it was found to have a similar pharmacokinetic profile to SCH 54429 (Table 2).

Structural evaluation using catalyst

The computer program Catalyst[12] has been used to generate a pharmacophore model (hypothesis) that attempts to correlate the biological activity observed for a series of compounds to their chemical structure. Pharmacophore models generated by the Catalyst program are three-dimensional representations of the chemical functions (hydrophobic groups, hydrogen-bond donors, hydrogen-bond acceptors, positive and negative ionizable groups, etc.) in a molecule that may participate in the binding interaction of the ligand at the receptor. The hypotheses generated may be used to

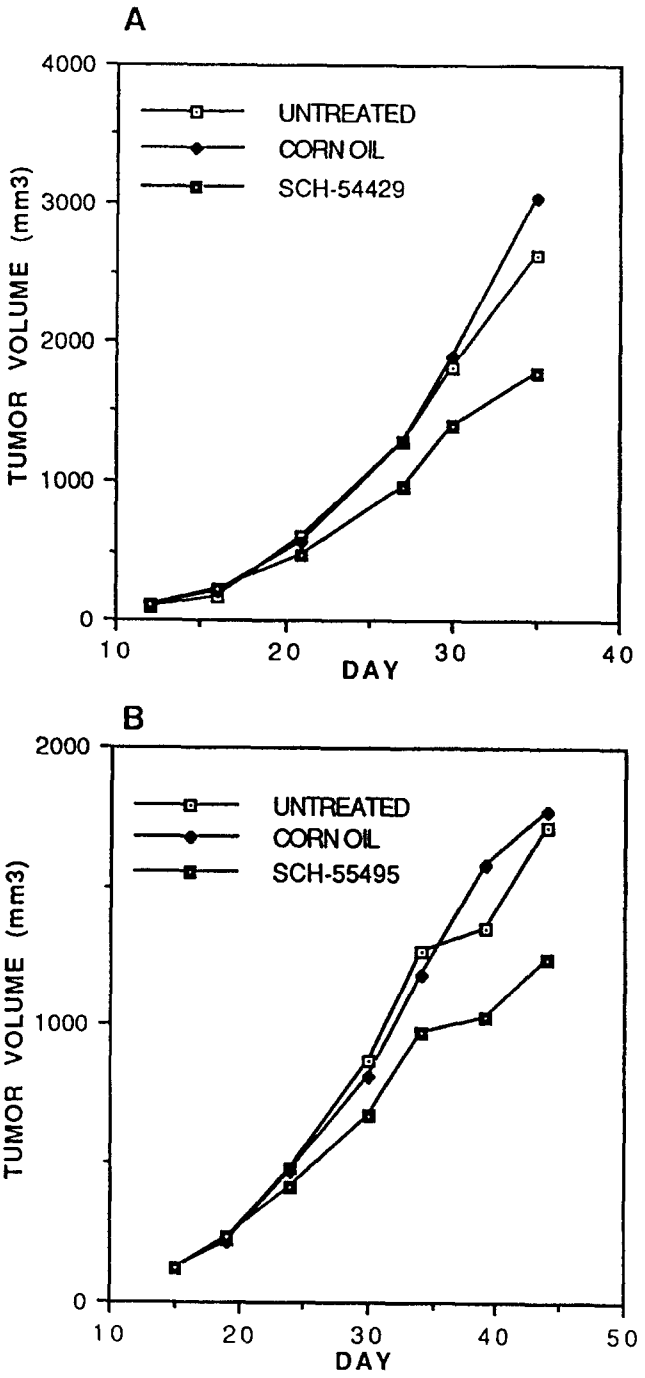

Figure 1. In vivo antitumor efficacy results. % tumor growth inhibition is the % change in tumor volume between the vehicle control group and the treated group and is measured on the last day of the assay. (a) SCH 54429 = 42%, (b) SCH 55495 = 30%.

estimate the biological activity of proposed targets allowing a rank ordering of synthetic priorities or to search three-dimensional databases of compounds to identify structurally novel analogues that might exhibit the biological activity of the prototype.

From the analogues prepared to investigate the SAR of this series, a training set of compounds was selected for Catalyst analysis which represented the diversity in the series based on the different chemical features present in their structures. The range of in vitro FPT inhibitory activity exhibited by these selected compounds spanned four orders of magnitude, i.e. $0.1-10^3$ μM.

Using this training set, an FPT hypothesis was generated (Fig. 2). This model consists of four hydrophobic regions and one hydrogen-bond acceptor in a particular three-dimensional orientation. The hydrogen-bond acceptor feature could also correspond to a zinc chelation site. Our FPT inhibitors map to this 'five-featured hypothesis' such that the four hydrophobic regions of the hypothesis include the pyridyl portion of the tricyclic system, the 5,6-ethano bridge of the tricyclic system, the chlorine atom in the 8-chlorophenyl portion of the tricyclic system, and the 4-pyridyl ring of the pyridylacetyl attached to the pendant piperylidenyl ring. The chiral compounds containing an *S*-configuration (SCH 69956) fits the pharmacophore model better than the compound containing an *R*-configuration (SCH 59955), which is consistent with the observed FPT activity (Table 1).

Since SCH 44342 kinetically competes with the ras protein but not with farnesyl pyrophosphate in binding to FPT,[9] we evaluated the structural similarities between our heterocyclic FPT inhibitors and a peptide inhibitor. The bound conformation of the tetrapeptide inhibitor CVWM (Cys-Val-Trp-Met) has been determined by NMR spectroscopy.[14] An ensemble of conformations for the peptide was generated using the published two-dimensional trNOE-derived distance constraints.[14] Although this peptide was not used in the training set for the pharmacophore model, the trNOE derived conformations do fit our Catalyst-generated pharmacophore model (Fig. 3). The lipophilic sidechains on valine, tryptophan and methionine bind to the lipophilic binding pockets and the methionine carboxyl group fits the hydrogen bonding pocket. Additional studies are needed to determine if our heterocyclic FPT inhibitors do in fact bind to FPT in a manner similar to peptides.

Conclusions

We have developed a novel class of heterocyclic, nonpeptidic, nonsulfhydryl inhibitors of ras farnesylation that act as antitumor agents when given orally to mice. Key structural features of the compounds described in this report, illustrated by the Catalyst-generated hypothesis shown in Figure 2, are critical for FPT potency. An SAR is developing and this information is being used to design improved FPT inhibitors. Further understanding of the metabolism and pharmacokinetics of these compounds should aid in the design of FPT inhibitors with superior antitumor efficacy.

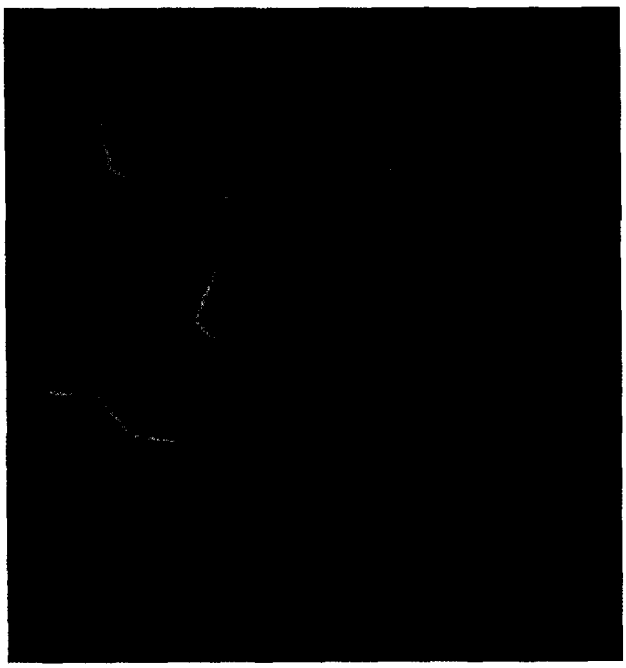

Figure 2. Low-energy conformations of SCH 44342 (blue), SCH 69956 (yellow), (*S*)-SCH 55495 (red) fit to the Catalyst FPT hypothesis. Hydrophobic regions cyan, hydrogen-bond acceptor region green.

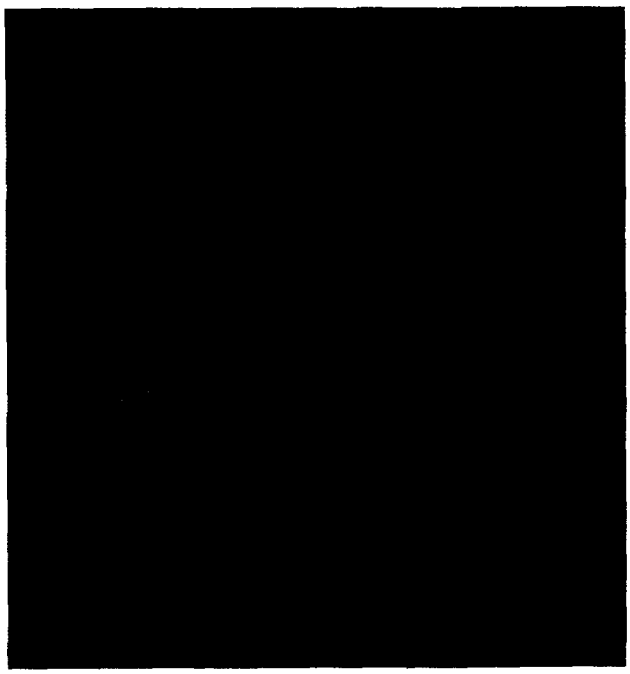

Figure 3. The conformation of CVWM bound to FPT consistent with reported NOE data fit to the Catalyst FPT hypothesis. Hydrophobic regions cyan, hydrogen-bond acceptor region green.

Experimental

Antitumor efficacy studies

SW-620 human colon adenocarcinoma tumor cells (7×10^6) containing a mutated K-ras oncogene, were injected subcutaneously into the flank of athymic nu/nu female mice, 6–7 weeks old (Charles River Laboratories, Wilmington, MA 01887). Drug treatment was initiated when the average tumor size exceeded 100 mm^3 (about 14 days post-inoculation), following the selection and randomization of tumor bearing mice. Five mice were assigned into each control and treatment group. The animals were dosed at 100 mg/kg, po bid for 5 days per week using a suspension of the drug in corn oil. Primary tumor measurements were determined twice a week, for a period of 5 weeks. Tumor volumes were calculated from caliper measurements of tumor dimensions in mm using the formula: tumor volume = 1/2 length × width × height. Efficacy of each compound is indicated by comparing the median tumor size of each treated group, at the end of the treatment, against the median tumor size of the vehicle control group.

Single-dose pharmacokinetic studies

Mice were given a single dose of SCH 44342 or SCH 54429 at 25 mg/kg by oral or iv administration as the HCl salt dissolved in saline. Blood samples were obtained by cardiac puncture under methoxyflurane anesthesia at specified time points up to 2 h post-dosing. Saline was isolated and 0.1 mL aliquots spiked with an internal standard (loratadine) and then extracted with 5 mL of 20% ethyl acetate in pentane. The organic layer was evaporated to dryness and the residue dissolved in 15 μL ethanol. A portion (1–2 μL) was injected onto a Varian 3500 Capillary Gas Chromatograph equipped with an autosampler, on-column injector and a capillary thermionic specific detector. Separation of the analyte and internal standard was achieved with a J&W DB-5 capillary column (15 m × 0.32 mm) using a temperature program (230–320 °C at 10 °C/min). Standard curves were prepared using drug-free mouse serum and appropriate amounts of SCH 44342 or SCH 54429. These standards were subjected to the same analytical procedure as the study samples. Peak height ratios of the analyte and internal standard were than plotted versus the concentration of analyte and least-squares linear regression ($1/Y$ weighting) performed to prepare calibration curves. SCH 44342 or SCH 54429 were quantitated in each study sample and used to calculate pharmacokinetic parameters. Serum half-lives were graphically estimated and the area under the concentration–time curve (AUC) was calculated using the linear trapezoidal rule.

8-Chloro-6,11-dihydro-11-(4-piperidinyl)-5*H*-benzo[5,6]cyclohepta[1,2-*b*]pyridine (2). To a mixture of 8-chloro-6, 11-dihydro-11- (4-piperidinylidene) -5H-benzo [5,6]cyclohepta[1,2-*b*]pyridine[17] (**1**, 29.3 g, 94 mmol) and anhyd tetrahydrofuran (420 mL) was slowly added lithium aluminum hydride (10.3 g, 0.27 mol). The resulting mixture was stirred at reflux for 3 h and then cooled to room temperature and combined with anhyd diethyl ether (1 L). Satd aq Na_2SO_4 was added dropwise until a precipitate formed. After 30 min, the solids were removed by filtration and the filtrate was dried over anhyd $MgSO_4$, filtered and concentrated in vacuo. The resulting residue was purified by flash column chromatography (silica gel) using 10% methanol (saturated with ammonia)–dichloromethane to provide 18.7 g of a white solid. This was found to be a mixture of the desired amine **2**, and the 8-deschloro derivative of **2**. This was used as is for the next step. ^{1}H NMR (200 MHz, $CDCl_3$): δ (ppm) 1.08–1.59 (m, 5H), 2.0–2.6 (m, 2H), 2.70–3.18 (m, 4H), 3.44 (m, 2H), 3.96 (m, 1H), 7.0–7.22 (m, 4H), 7.40 (br d, 1H, J = 7 Hz), 8.35 (d, 1H, J = 5 Hz); IR (KBr): 3230, 2932, 2810, 1560, 1430 cm^{-1}; MS - SIMS: m/z 379 (MH^+, 60%), 313 (MH^+, 100%).

4-[8-Chloro-6,11-dihydro-5*H*-benzo[5,6]cyclohepta[1,2-*b*]pyridin-11-yl]-1-(4-pyridinylacetyl)-piperidine (SCH 55495). The above mixture of **2** and the 8-deschloro derivative of **2** (4.42 g, 14 mmol), 4-pyridylacetic acid hydrochloride (2.70 g, 16 mmol), 1-(3-dimethylaminopropyl)-3-ethyl carbodiimide hydrochloride (4.06 g, 21 mmol), 1-hydroxybenzotriazole (1.91 g, 14 mmol), 4-methylmorpholine (9.3 mL, 85 mmol) and anhyd dimethylformamide (125 mL) was stirred at room temperature under N_2 for 48 h. The reaction mixture was concentrated in vacuo and the resulting residue was purified by flash column chromatography (silica gel) using 4% methanol–dichloromethane saturated with ammonia to provide 4.3 g of a white solid. This was found to contain 70% of the desired SCH 55495 and 30% of the 8-deschloro derivative, which were separated using reverse-phase HPLC (C-18) and 37% methanol–63% water (containing 0.1% TFA) as eluent to give SCH 55495 (the second peak) as a white solid; mp 94.4–95 °C; ^{1}H NMR (200 MHz, $CDCl_3$): δ (ppm) 0.9–1.63 (m, 4H), 2.47 (m, 2H), 2.93 (m, 3H), 3.40 (m, 2H), 3.63–4.04 (m, 2H), 3.70 (overlapping s, 2H), 7.0–7.35 (m, 6H), 7.40 (br d, 1H, J = 8 Hz), 8.35 (br d, 1H, J = 5 Hz), 8.55 (d, 1H, J = 5 Hz); IR (KBr): 3440, 2939, 1630, 1440 cm^{-1}; MS - SIMS: m/z 432 (MH^+, 100%). Anal. calcd for $C_{26}H_{26}N_3OCl \cdot 0.45H_2O$: C, 70.91; H, 6.11; N, 9.54; found: C, 70.91; H, 6.37; N, 9.42.

(+)-8-Chloro-6,11-dihydro-11(*R*)-(1-piperazinyl)-5*H*-benzo[5,6]cyclohepta[1,2-*b*]pyridine (4). 8-Chloro-6,11-dihydro-11-(1-piperazinyl)-5*H*-benzo[5,6]cyclohepta[1,2-*b*]pyridine,[16] **3** (88 g, 0.28 mol) was dissolved in 900 mL of 8% water in acetonitrile and warmed on a steam bath. A solution of 49 g (0.28 mol) of (−)-L-*N*-acetylleucine dissolved in 1600 mL of hot 8% aq acetonitrile was then added and the solution was allowed to cool to room temperature. The resulting crystals were filtered and again crystallized from 1300 mL of hot 8% aq acetonitrile. The resulting crystals (mp = 234–236 °C) were filtered, dissolved in 1.5 L of dichloromethane and adjusted to pH 8 with aq potassium carbonate

solution. The organic layer was washed with brine, dried over sodium sulfate, filtered and concentrated in vacuo giving 23 g (52% yield) of the *R*(+)-enantiomer as a white solid, mp = 153–155 °C, $[\alpha]_D^{22}$ +66° (*c* 0.5, methanol). The optical purity was 94% e.e. as determined by HPLC using a 4.6 mm × 250 mm Chiralcel-OD column eluting with cyclohexane:2-propanol: diethylamine (85:15:0.1) at a flow rate of 1.0 mL/min and detecting at 268 nm. For structural proof of the absolute configuration, see the preparation of the *S*(−)- enantiomer described below.

(−)-8-Chloro-6,11-dihydro-11(*S*)-(1-piperazinyl)-5*H*-benzo[5,6]cyclohepta[1,2-*b*]pyridine (5). The second filtrate from the above resolution of the *R*(+)-enantiomer was concentrated in vacuo. The resulting residue was dissolved in 1.5 L of dichloromethane and adjusted to pH 8 with aq potassium carbonate solution. The organic layer was washed with brine, dried over sodium sulfate, filtered and concentrated in vacuo giving the 43 g of a white solid. This was resolved as above for the *R*(+)-enantiomer using 16 g of (+)-D-*N*-acetylleucine giving 16.6 g of the product as a white solid, mp = 153–155 °C, $[\alpha]_D^{22}$ −68° (*c* 0.5, methanol). The optical purity was 98% e.e., as determined by the above HPLC method. The absolute configuration was determined to be (*S*) by X-ray crystallography on the (+)-D-*N*-acetylleucine salt.[18]

1-(8-Chloro-6,11-dihydro-5*H*-benzo[5,6]cyclohepta[1,2-*b*]pyridin-11-yl)-4-(4-pyridinylacetyl)piperazine (SCH 54429). 8-Chloro-6,11-dihydro-11-(1-piperazinyl)-5*H*-benzo[5,6]cyclohepta[1,2-*b*]pyridine,[16] **3** (8.53 g, 27 mmol), 4-pyridylacetic acid (3.72 g, 27 mmol), 1-(3-dimethylaminopropyl)-3-ethylcarbodiimide hydrochloride (7.81 g, 27 mmol), 4-methylmorpholine (2.99 mL, 27 mmol) and 1-hydroxybenzotriazole (3.68 g, 27 mmol) were dissolved in anhyd dimethylformamide (256 mL) and the mixture was stirred under argon at 25 °C for 18 h. The mixture was diluted with dichloromethane and washed with water. The dichloromethane layer was dried (magnesium sulfate) and evaporated to dryness. Chromatography on a silica gel column (120 × 8 cm) using 1.5% (10% concd ammonium hydroxide in methanol)–dichloromethane (4 L), followed by 2.5% (8 L) and then 3.0% of the above solvent system afforded SCH 54429 as a white amorphous solid (8.67 g, 74%). Found: C, 68.15; H, 5.64; Cl, 8.00; N, 12.51. $C_{25}H_{25}Cl\ N_4O$ requires: C, 69.35; H, 5.82; Cl, 8.19; N, 12.94%. CIMS: *m/z* 433 (MH^+), δ_H ($CDCl_3$) 3.68 (2H, s, CH_2), 4.36 (IH, H_{11}), 7.11 (IH, m, Ar-H), 7.16 (5H, m, Ar-H), 7.45 (1H, m, Ar-H), 8.34 (1H, m, Ar-H) and 8.55 (2H, m, Ar-H).

(+)-1-(8-Chloro-6,11-dihydro-5*H*-benzo[5,6]cyclohepta[1,2-*b*]pyridin-11(*R*)-yl)-4-(4-pyridinylacetyl)piperazine (SCH 69955). (+)-8-Chloro-6,11-dihydro-11(*R*)-(1-piperazinyl)-5*H*-benzo[5,6]cyclohepta[1,2-*b*]pyridine, **4** (500 mg, 1.6 mmol), 4-pyridylacetic acid (328 mg. 2.61 mmol), 1-(3-dimethylaminopropyl)-3-ethylcarbodiimide hydrochloride (458.2 mg. 2.4 mmol), 4-methylmorpholine, (0.263 mL, 2.4 mmol) and 1-hydroxybenzotriazole (323 mg, 2.4 mmol) were dissolved in anhyd dimethylformamide (15 mL) and the mixture was stirred under argon at 25 °C for 69 h. The mixture was diluted with dichloromethane and washed with 1 N aq sodium hydroxide. The dichloromethane layer was dried (magnesium sulfate) and evaporated to dryness. Chromatography on a silica gel column (60 × 2.5 cm) using 3% (10% concd ammonium hydroxide in methanol)–dichloromethane as the eluant afforded SCH 69955 as a white amorphous solid (650.9 mg, 94%). Found: C, 68.71; H, 6.46; Cl, 8.12; N, 12.71. $C_{25}H_{25}ClN_4O$ requires: C, 69.30; H, 5.82; Cl, 8.19; N, 12.94%). CIMS: *m/z* 433 (MH^+), $[\alpha]_D^{25}$ = +39.8° (*c* 0.5, methanol), δ_H ($CDCl_3$) 3.67 (2H, s, CH_2), 4.34 (1H, s, H_{11}), 7.09 (IH, m, Ar-H), 7.14 (5H, m, Ar-H), 7.43 (1H, m, Ar-H), 8.32 (1H, m, Ar-H) and 8.54 (2H, m, Ar-H).

(−)-1-(8-Chloro-6,11-dihydro-5*H*-benzo[5,6]cyclohepta[1,2-*b*]pyridin-11(*S*)-yl)-4-(4-pyridinylacetyl)piperazine (SCH 69956). (−)-8-Chloro-6,11-dihydro-11(*S*)-(1-piperazinyl)-5*H*-benzo[5,6]cyclohepta[1,2-*b*]pyridine, **5** (500 mg, 1.6 mmol), 4-pyridylacetic acid (328 mg, 2.4 mmol), 1-(3-dimethylaminopropyl)-3-ethylcarbodiimide hydrochloride (458.2 mg, 2.4 mmol), 4-methylmorpholine (0.263 mL, 2.4 mmol) and 1-hydroxybenzotriazole (323 mg, 2.4 mmol) were dissolved in anhyd dimethylformamide (15 mL) and the mixture was stirred under argon at 25 °C for 69 h. The mixture was diluted with dichloromethane and washed with 1 N aq sodium hydroxide. The dichloromethane layer was dried (magnesium sulfate) and evaporated to dryness. Chromatography on a silica gel column (60 × 2.5 cm) using 3% (10% concd ammonium hydroxide in methanol)–dichloromethane as the eluant afforded SCH 69955 as a white amorphous solid (533.4 mg, 77%). Found: C, 68.61; H, 6.20; Cl, 8.26; N, 12.77. $C_{25}H_{25}ClN_4O$ requires: C, 69.30; H, 5.82; Cl, 8.19; N, 12.94%), CIMS: *m/z* 433 (MH^+), $[\alpha]_D^{25}$ −41.6° (*c* 0.5, methanol), δ_H ($CDCl_3$) 3.68 (2H, s, CH_2), 4.34 (1H, s, H_{11}), 7.10 (IH, m, Ar-H), 7.14 (5H, m, Ar-H), 7.43 (1H, m, Ar-H), 8.32 (1H, m, Ar-H) and 8.53 (2H, m, Ar-H).

4-[8-Chloro-5,6-dihydro-11*H*-benzo[5,6]cyclohepta[1,2-*b*]pyridin-11-ylidene]-1-[2-[(4-pyridinyl)acetyl]]piperidine (SCH 50739). To a cooled (0 °C) solution of 8-chloro-6,11-dihydro-11-(4-piperidinylidene)-5*H*-benzo[5,6]cyclohepta[1,2-*b*]pyridine[17] **1** (0.8 g, 4 mmol), and triethylamine (0.6 mL, 4 mmol) in dichloromethane (50 mL) was added 4-(2-bromoacetyl)pyridine (1.03 g, 3.3 mmol). After stirring for 1.5 h, the mixture was diluted with dichloromethane and washed with a saturated solution of aq sodium bicarbonate and brine. The organic phase was dried over anhyd sodium sulfate, filtered and concentrated in vacuo. The resulting residue was purified by flash column chromatography (silica gel) using 2% methanol–dichloromethane as eluent to provide the product as a glass (0.59 g, 53% yield). An analytical sample was prepared by flash column chromatography (silica gel) using 2–3% methanol–dichloromethane as eluent: glass; ^1H

NMR (300 MHz, $CDCl_3$): δ (ppm) 2.32–2.70 (m, 6H), 2.87 (m, 4H), 3.42 (m, 2H), 3.82 (s, 2H), 7.1–7.23 (m, 4H), 7.48 (dd, 1H, $J=7$, 1 Hz), 7.82 (br d, 2H, $J=7$ Hz), 8.43 (dd, 1H, $J=5$, 1 Hz), 8.83 (br d, 2H, $J=7$ Hz); FABMS: *m/z* 430 (MH^+, 6%), 311 (100%). Anal. calcd for $C_{26}H_{24}N_3OCl \cdot 0.4H_2O$: C, 71.16; H, 5.70; N, 9.57. Found: C, 71.32; H, 5.51; N, 9.58.

References

1. Barbacid, M. *Annu. Rev. Biochem.* **1987**, *56*, 779.
2. Hall, A. *Science* **1994**, *264*, 1413.
3. Rodenhuis, S. *Semin. Cancer Biol.* **1992**, *3*, 241.
4. Casey, P. J.; Solski, P. A.; Der, C. J.; Buss, J. E. *Proc. Natl. Acad. Sci. U.S.A.* **1989**, *86*, 8323.
5. Zhang, F. L.; Casey, P. J. *Annu. Rev. Biochem.* **1996**, *65*, 241.
6. Graham, S. L. *Exp. Opin. Ther. Patents* **1995**, *5*, 1269.
7. Sepp-Lorenzino, L.; Ma, Z.; Rands, E.; Kohl, N. E.; Gibbs, J. B.; Oliff, A.; Rosen, N. *Cancer Res.* **1995**, *55*, 5302.
8. Nagasu, T.; Yoshimatsu, K.; Rowell, C.; Lewis, M. D.; Garcia A, M. *Cancer Res.* **1995**, *55*, 5310.
9. Bishop, W. R.; Bond, R.; Petrin, J.; Wang, L.; Patton, R.; Doll, R.; Njoroge, G.; Catino, J.; Schwartz, J.; Windsor, W.; Syto, R.; Schwartz, J.; Carr, D.; James, L.; Kirschmeier, P. *J. Biol. Chem.* **1995**, *270*, 30611.
10. Yokoyama, K.; Gelb, M. H. *J. Biol. Chem.* **1993**, *268*, 4055.
11. Seabra, M. C.; Goldstein, J. L.; Sudhof, T. C.; Brown, M. S. *J. Biol. Chem.* **1992**, *267*, 14497.
12. Catalyst v2.1 Molecular Simulations, Inc., Burlington, MA.
13. Stradley, S. J.; Rizo, J.; Gierasch, L. *Biochemistry* **1993**, *32*, 12586.
14. Koblan, K. S.; Culberson, J. C.; Desolms, S. J.; Giuliani, E. A.; Mosser, S. D.; Omer, C. A.; Pitzenberger, S. M.; Bogusky, M. J. *Protein Sci.* **1995**, *4*, 681.
15. Piwinski, J. J.; Ganguly, A. K.; Green, M. J.; Villani, F. J.; Wong, J. U.S. Patent: 5,089,496, 18 February, 1992.
16. Piwinski, J. J.; Green, M. J.; Wong, J. U.S. Patent: 5,422,351, 6 June, 1995.
17. Piwinski, J. J.; Ganguly, A. K.; Green, M. J.; Villani, F. J.; Wong, J. U.S. Patent: 4,826,853, 2 May, 1989.
18. Wong, J.; McPhail, A. T. Unpublished data.

(*Received in U.S.A.* 1 *April* 1996; *accepted* 2 *May* 1996)